

# Electronic and optical properties of families of polycyclic aromatic hydrocarbons: a systematic (time-dependent) density functional theory study

G. Mallocci<sup>a,\*</sup>, G. Cappellini<sup>a,b</sup>, G. Mulas<sup>b</sup>, A. Mattoni<sup>a</sup>

<sup>a</sup>*CNR-IOM and Dipartimento di Fisica, Università degli Studi di Cagliari, Cittadella Universitaria, Strada Prov. le Monserrato-Sestu Km 0.700, I-09042 Monserrato (CA), Italy*

<sup>b</sup>*INAF – Osservatorio Astronomico di Cagliari–Astrochemistry Group, Strada 54, Località Poggio dei Pini, I-09012 Capoterra (CA), Italy*

---

## Abstract

Homologous classes of Polycyclic Aromatic Hydrocarbons (PAHs) in their crystalline state are among the most promising materials for organic opto-electronics. Following previous works on oligoacenes we present a systematic comparative study of the electronic, optical, and transport properties of oligoacenes, phenacenes, circumacenes, and oligorylenes. Using density functional theory (DFT) and time-dependent DFT we computed: (i) electron affinities and first ionization energies; (ii) quasiparticle correction to the highest occupied molecular orbital (HOMO)-lowest unoccupied molecular orbital (LUMO) gap; (iii) molecular reorganization energies; (iv) electronic absorption spectra of neutral and  $\pm 1$  charged systems. The excitonic effects are estimated by comparing the optical gap and the quasiparticle corrected HOMO-LUMO energy gap. For each molecular property computed, general trends as a function of molecular size and charge state are discussed. Overall, we find that circumacenes have the best transport properties, displaying a steeper decrease of the molecular reorganization energy at increasing sizes, while oligorylenes are much more efficient in absorbing low-energy photons in comparison to the other classes.

*Key words:* PAHs, Electronic absorption, Charge-transport, Density functional theory, Time-dependent density functional theory

---

\* Corresponding author. Tel: +39-070-675-4839; Fax: +39-070-510171  
*Email address:* giuliano.mallocci@dsf.unica.it (G. Mallocci).

## 1 Introduction

A large class of conjugated  $\pi$ -electron systems, polycyclic aromatic hydrocarbons (PAHs) are of fundamental importance in many research areas of chemistry as well as in materials science and astrophysics. PAHs are precursors of extended carbon networks [1a,1b] and their carbon skeletons can be seen as small pieces of graphene [2a,2b]. Some PAHs are of interest in environmental chemistry due to their carcinogenicity and their ubiquity as air pollutants produced by the combustion of organic matter [3a,3b]. Neutral and charged PAHs up to large sizes are thought to be abundant in space and are thus seen as an intermediate stage between the gas and dust phases of the matter between stars [4a,4b].

Homologous classes of PAHs in their crystalline state are among the most promising materials for organic electronics [5]. Oligoacenes and their derivatives, for example, are being increasingly used as active elements in a variety of opto-electronic devices such as organic thin-film field-effect transistors [6], light-emitting diodes [7], photovoltaic cells [8], and liquid crystals [9]. Organic electronics based on functionalized acenes and heteroacenes is presently a very active field of research [10a,10b,10c,10d,10e].

The main features controlling organic semiconducting devices are exciton formation, migration, and dissociation, charge transport, charge collection at the electrodes, molecular packing in the bulk material, and absorption and emission properties [14a,14b]. Since many of these properties pertain mostly to the molecular units, systematic quantum-chemical calculations on isolated PAHs can significantly contribute to our understanding of the electronic and optical properties of families with promising opto-electronic applications.

As a part of a more extensive research on PAHs [15], and following our previous work on oligoacenes [16a,16b], we present in this paper a comprehensive comparative theoretical study of four homologous classes of PAHs, namely oligoacenes, phenacenes, circumacenes, and oligorylenes, in their neutral, cationic, and anionic charge-states. This choice of families was motivated by the availability of reliable experimental data for the first members of each class. They include both catacondensed (oligoacenes and phenacenes) and pericondensed (circumacenes and oligorylenes) species, spanning a representative range of regular, relatively symmetric PAHs. Moreover circumacenes and oligorylenes converge, at the infinite limit, to a zigzag and arm-chair edged graphene nanoribbon, respectively, and as such are promising candidates for organic and molecular electronics [13]. We restricted ourselves to the first five members of each class.

The geometries of the molecules considered are sketched in Fig. 1. Oligoacenes

[5] and phenacenes [11] consist of fused benzene rings joined in a linear and zig-zag arrangement, respectively. Oligorylenes [12] can be seen as a series of naphthalene molecules connected by two carbon-carbon bonds, and circumacenes are obtained by addition of benzene units around the circumference of their oligoacenes counterparts. Note that, with the exception of circumtetracene, circumpentacene, and hexarylene, all of the molecules considered have been synthesized.

We used density functional theory (DFT) [17a,17b,17c,17d] to compute the electronic ground-state of the molecules considered, and time-dependent DFT (TD-DFT) [18a,18b,18c,18d] to obtain their electronic absorption spectra. To the best of our knowledge the complete photo-absorption spectra of higher neutral and charged phenacenes, circumacenes, and oligorylenes are reported here for the first time. The knowledge of this property, in particular, enabled a comparison of the absorption in the visible part of the spectrum, a quantity of interest for photovoltaic applications. Moreover, we used total-energy differences between the self-consistent field calculations performed for the neutral and charged systems ( $\pm 1$ ) to evaluate: (i) the vertical and adiabatic electron affinities and first ionization energies; (ii) the quasiparticle correction to the highest occupied molecular orbital (HOMO)-lowest unoccupied molecular orbital (LUMO) gap; (iii) the molecular reorganization energies. The comparison between the optical gap, i.e. the lowest singlet-singlet TD-DFT excitation energy, and the quasiparticle corrected HOMO-LUMO gap enabled a rough estimate of the excitonic effects occurring in these molecules.

The paper is organized as follows. Section 2 reports some technical details of the calculations. The results we obtained are presented and discussed in Sect. 3. Our concluding remarks are reported in Sect. 4.

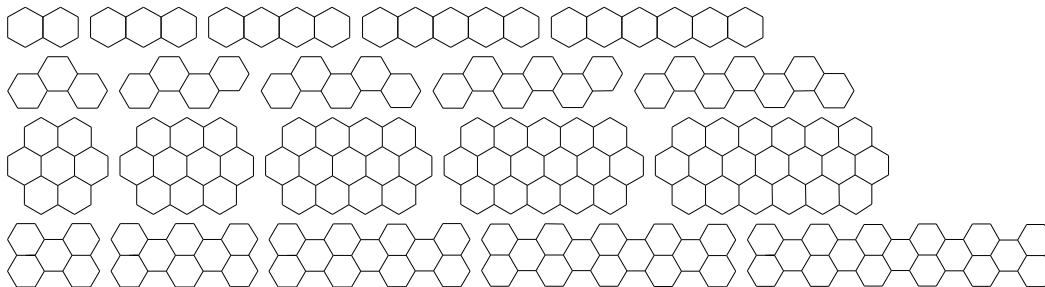


Fig. 1. Oriented geometries of the molecules considered. From top to bottom: oligoacenes (naphthalene, anthracene, tetracene, pentacene, hexacene), phenacenes (phenanthrene, chrysene, picene, fulminene, 7-phenacene), circumacenes (coronene, ovalene, circumanthracene, circumtetracene, circumpentacene), and oligorylenes (perylene, terrylene, quaterrylene, pentarylene, hexarylene).

## 2 Computational details

### 2.1 Geometry optimizations

We used the Gaussian-based DFT module of the NWChem package [19] to compute the ground-state properties of each molecule in its  $-1, 0, +1$  charge-state. Following our previous studies on linear acenes [16a,16b], we used a basis-set with the smallest addition of diffuse functions, namely the 6-31+G\* basis, a valence double zeta set augmented with  $d$  polarization functions and  $s$  and  $p$  diffuse functions for each carbon atom. Geometry optimizations were performed using tight convergence criteria, specified by maximum and root mean square gradient thresholds of  $1.5 \cdot 10^{-5}$  and  $1.0 \cdot 10^{-5}$  atomic units, respectively, and maximum and root mean square thresholds of the Cartesian step respectively of  $6.0 \cdot 10^{-5}$  and  $4.0 \cdot 10^{-5}$  atomic units. All neutral and singly-charged species were computed as singlet and doublet, respectively, which are known to be the ground states for this class of molecules [22b,23a,23c].

Geometry optimization were performed using the hybrid B3LYP functional, a combination of the Becke's three parameter exchange functional [20] and the Lee-Yang-Parr gradient-corrected correlation functional [21]. In comparison with other exchange-correlation functionals, the B3LYP has proven to give results markedly more accurate for the ground-state properties of PAHs [22a,22b] and has been used in a large number of studies [23a,23b,23c,23d,23e,23f,23g,23h,23i,23j,23k]. Although the B3LYP functional has been developed for the electronic ground-state, it is also routinely employed to obtain electronic excited-state properties, and its application usually yields accurate results for low-lying valence-excited states of both closed-shell [24a,24b] and open-shell [25a,25b] species. It is known, however, that this functional show the wrong asymptotic behaviour, decaying faster than  $1/R$  (i.e., exponentially) for large distances  $R$  from the nuclei. Among the well known and documented limitations of conventional functionals [18d] are: (i) the correct description of Rydberg [26a,26b,26c], doubly-excited [27a,27b], and charge-transfer [28a,28b,28c] excited-states, (ii) the failure for large, extended  $\pi$ -systems such as polyacetylene fragments and oligoporphyrins [29], and (iii) the system-size-dependent errors found for the lowest short-polarized excited states of neutral oligoacenes [23f].

This latter error in particular, which is particularly relevant to the present study, was recently shown to be corrected by range-separated functionals [30]. While conventional hybrid functional such as B3LYP are defined with a constant fraction of Hartree-Fock exchange, the authors of Ref. [30] used range-separated functionals [31a,31b,31c,31d] incorporating both a position-dependent fraction and an asymptotically correct contribution of Hartree-Fock exchange. The application of range-separated functionals to organic compounds show

that they provide, in general, a better accuracy than global hybrids [32a,32b,32c,32d,32e].

As to the molecular properties of interest in this work (electron affinities, ionization energies, quasiparticle corrected HOMO–LUMO gaps, exciton binding energy, electronic excitations), we recently checked for oligoacenes both the sensitivity of our calculations to different exchange–correlation functionals [33a,33b], and their reliability in comparison with the available experimental data. With the only exception of the ionization energy, which were found to be described better at the LDA level, we found that the hybrid B3LYP functional yields the overall best performance. To further assess this choice we performed some benchmark calculations using the range separated functional LC–BLYP [32e], which was found to give the best results in describing the optoelectronic properties of oligoacenes [30]. Table 1 reports the comparison between B3LYP, LC–BLYP, and the available experimental data of oligoacenes. A similar comparison for some selected properties for which we could find the corresponding experimental data is presented in Table 2 for the smallest species of the four PAH families considered, namely naphthalene, phenanthrene, coronene, and perylene.

The results in Table 1 are consistent with those reported in Ref. [30], the small differences being due to the larger basis set *cc*-PVTZ used in the latter work. As shown by the reported mean absolute errors (MAE) and root-mean-squared errors (RMS), the use of LC–BLYP is indeed (i) able to solve the system–size–dependent errors of B3LYP found for the lowest excited state corresponding to the HOMO–LUMO transition (*p* bands); (ii) gives ionization energies that are in much more agreement than B3LYP with experiments; and (iii) provides better quasiparticle corrected HOMO–LUMO gaps. At the same time, however, the B3LYP functional appears to outperform LC–BLYP with respect to the  $\alpha$  and  $\beta$  bands, the electron affinity, and the exciton binding energy; the molecular reorganization energies are described with the same accuracy by the two methods. When considering different families as done in Table 2, the B3LYP results are always in better agreement with experiments, with the only exception of the ionization energy. Since definitive conclusions cannot be drawn from our benchmark calculations and a thorough comparison between the performances of global hybrids and range–separated functionals is beyond the scope of this work, we decided to extend our previous analyses for oligoacenes [16a,16b], using the same level of theory B3LYP/6–31+G\* for the other classes of PAHs considered in this work.

## 2.2 *Total–energy differences calculations*

From the structural relaxations performed for both neutral and charged systems, we computed via total–energy differences the adiabatic electron affinities

Table 1

Comparison between B3LYP, LC-BLYP, and the available experimental data of oligoacenes (number of benzene rings from 2 to 6). The three lowest electronic transitions (usually described by Clars’s notation  $p$ ,  $\alpha$ ,  $\beta$ ) are computed by means of linear response TD-DFT (see Sect. 2.3). Ionization energies, electron affinities ionization energy, quasi-particle corrected HOMO-LUMO gaps, exciton binding energy, and molecular reorganization energy are computed via total energy differences (see Sect. 2.2). The experimental data are taken from the compilation in Ref. [16a] with the exception of the molecular reorganization energies  $\lambda$  taken from Ref. [14b]. The last rows report the mean absolute errors (MAE) and root-mean-squared errors (RMS) for each quantity; all values are given in eV.

n	Method	$p$	$\alpha$	$\beta$	IE	EA	QP	$E_{\text{bind}}$	$\lambda$
2	B3LYP	4.36	4.44	5.85	7.89	-0.38	8.27	3.91	0.178
	LC-BLYP	4.82	4.60	6.07	8.13	-0.42	8.55	3.95	0.217
	EXP	4.45	3.97	5.89	8.144	-0.20	8.34	3.89	0.182
3	B3LYP	3.21	3.85	5.14	7.09	0.43	6.66	3.45	0.134
	LC-BLYP	3.72	4.04	5.42	7.34	0.39	6.95	3.23	0.173
	EXP	3.45	3.84	5.24	7.439	0.53	6.91	3.46	0.174
4	B3LYP	2.45	3.47	4.62	6.55	1.00	5.55	3.10	0.109
	LC-BLYP	2.98	3.67	4.95	6.80	0.96	5.85	2.87	0.150
	EXP	2.72	3.12	4.55	6.970	1.067	5.90	3.18	0.138
5	B3LYP	1.91	3.21	4.24	6.16	1.41	4.75	2.84	0.092
	LC-BLYP	2.44	3.42	4.60	6.42	1.37	5.05	2.61	0.133
	EXP	2.31	3.73	4.40	6.589	1.392	5.20	2.89	0.102
6	B3LYP	1.51	3.02	—	5.87	—	—	—	—
	LC-BLYP	2.00	3.20	—	6.13	—	—	—	—
	EXP	1.90	2.80	—	6.360	—	—	—	—
MAE (RMS)	B3LYP	0.28 (0.13)	0.31 (0.16)	0.09 (0.05)	0.39 (0.18)	0.09 (0.05)	0.28 (0.16)	0.04 (0.02)	0.02 (0.01)
	LC-BLYP	0.23 (0.11)	0.42 (0.20)	0.24 (0.13)	0.14 (0.07)	0.12 (0.07)	0.11 (0.07)	0.22 (0.12)	0.02 (0.01)

and the adiabatic single ionization energies. At the optimized geometry of the neutral molecule we then evaluated the vertical electron affinity ( $EA_v$ ) and the vertical first ionization energy ( $IE_v$ ). This enabled the calculation of the quasiparticle-corrected HOMO-LUMO gap of the neutral systems; this quantity is usually referred to as the fundamental gap and is rigorously defined

Table 2

Same as in Table 1 for the smallest species of each PAH family considered; the experimental data are taken from the references given in Tables 3-4.

Molecule	Method	$p$	IE	EA	QP	$E_{\text{bind}}$
Naphthalene	B3LYP	4.36	7.89	-0.38	8.27	3.91
	LC-BLYP	4.82	8.13	-0.42	8.55	3.95
	EXP	4.45	8.144	-0.20	8.34	3.89
Phenanthrene	B3LYP	4.19	7.63	-0.21	7.84	3.65
	LC-BLYP	4.30	7.92	-0.29	8.20	3.90
	EXP	4.24	7.891	0.01	7.88	3.64
Coronene	B3LYP	3.42	7.08	0.38	6.70	3.28
	LC-BLYP	3.52	7.41	0.27	7.15	3.63
	EXP	3.74	7.290	0.47	6.82	3.08
Perylene	B3LYP	2.79	6.64	0.87	5.77	2.98
	LC-BLYP	3.26	6.92	0.81	6.11	2.85
	EXP	2.82	6.960	0.973	5.99	3.17
MAE (RMS)	B3LYP	0.12 (0.08)	0.26 (0.13)	0.15 (0.08)	0.11 (0.07)	0.10 (0.07)
	LC-BLYP	0.27 (0.15)	0.05 (0.03)	0.22 (0.11)	0.25 (0.13)	0.30 (0.17)

within the  $\Delta$ SCF scheme [17b] as:

$$\text{QP}_{\text{gap}}^1 = \text{IE}_v - \text{EA}_v = E_{N+1} + E_{N-1} - 2E_N, \quad (1)$$

$E_N$  being the total energy of the  $N$ -electron system. We used also the following approximate expression [17a]:

$$\text{QP}_{\text{gap}}^2 = \epsilon_{N+1}^{N+1} - \epsilon_N^N, \quad (2)$$

where  $\epsilon_i^j$  is the  $i^{\text{th}}$  Kohn–Sham eigenvalue of the  $j$ -electron system. The results obtained using the above Eqs. (1) and (2) tend to coincide as the system gets larger and the orbitals more delocalized.

Concerning transport properties, in organic molecular semiconductors conductivity is known to occur via a hopping mechanism in which charge carriers jump between adjacent molecules, usually under the effect of an external ap-

plied field. This process can be described by the semiclassical Marcus theory of electron transfer with overall rate constant proportional to  $\exp[-\lambda/(4K_{\text{B}}T)]$  ( $K_{\text{B}}$  Boltzmann’s constant,  $T$  temperature) [14a,14b]. The quantity  $\lambda$ , the molecular reorganization energy or intramolecular coupling, affects critically the charge–transfer process: low values of the reorganization energy imply high transfer rates.  $\lambda$  can be computed via the ”four–point method” as the sum of two contributions [14a,14b]:

$$\lambda = \lambda_1 + \lambda_2 = (E_+^* - E_+) + (E^* - E). \quad (3)$$

In the equation above,  $E$  and  $E_+$  are the total energies of the neutral and cation in their equilibrium structures, respectively,  $E_+^*$  is the total energy of the cation in the neutral geometry, and  $E^*$  is the total energy of the neutral in the cation geometry. While the first term  $\lambda_1$  corresponds to the radical cation formation, the second one  $\lambda_2$  accounts for the relaxation of the charged state.

### 2.3 TD–DFT calculations

To compute the excitation energies and electronic absorption spectra we used two different implementations of TD–DFT in the linear response regime, in conjunction with different representations of the wavefunctions:

- (1) the frequency–space implementation [18a] based on the linear combination of localized orbitals, as given in the NWCHEM package [19];
- (2) the real–time propagation scheme using a grid in real space [18b], as implemented in the OCTOPUS computer program [35a,35b].

We used the scheme (1) at the same level B3LYP/6-31+G\* used to obtain the ground–state geometries and restricted ourselves to the first few singlet–singlet electronic transitions. In scheme (2) one obtains the whole absolute photo–absorption cross–section  $\sigma(E)$  from the dynamical polarizability  $\alpha(E)$  through the equation:

$$\sigma(E) = \frac{8\pi^2 E}{hc} \Im\{\alpha(E)\}, \quad (4)$$

where  $h$  is Planck’s constant,  $\Im\{\alpha(E)\}$  is the imaginary part of the dynamical polarizability, and  $c$  is the velocity of light in vacuum. The dipole strength–function  $S(E)$  is related to  $\sigma(E)$  by the equation:

$$S(E) = \frac{m_e c}{\pi \hbar e^2} \sigma(E), \quad (5)$$

$m_e$  and  $e$  being respectively the mass and charge of the electron.  $S(E)$  has units of oscillator strength per unit energy and satisfies the Thomas–Reiche–Kuhn dipole sum–rule  $N_e = \int dE S(E)$ , where  $N_e$  is the total number of electrons. The real–time TD–DFT method in real space was proven to give good results for PAHs up to photon energies of about 30 eV [16a,16b]. For the calculations performed with OCTOPUS we used the same prescription as in Ref. [16a].

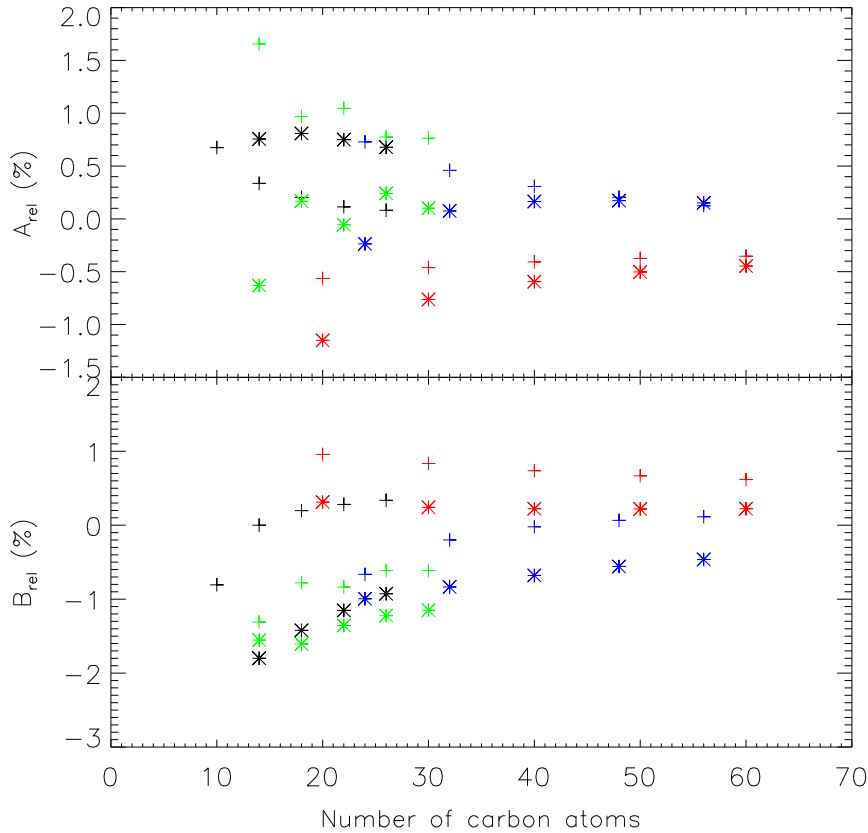


Fig. 2. Percentage variation of the rotational constants A (top panel) and B (bottom panel) relative to the neutral counterparts for anions (asterisks) and cations (crosses), as a function of molecular size for oligoacenes (black), phenacenes (green), circumacenes (blue), and oligorylenes (red). We omit the entries for naphthalene anion, which is known not to form a stable anion in the gas–phase.

### 3 Results and discussion

#### 3.1 Geometry optimization

In our previous studies [16a,16b] we found that the structural parameters obtained for ionized oligoacenes, ignoring any apparent symmetry and adopting the  $D_{2h}$  symmetry of the corresponding neutral molecule, are coincident within numerical errors. We therefore assumed in this work the same symmetry of the neutral molecule for each charged species considered, with the exception of coronene anion and cation, which are known to undergo Jahn–Teller distortion from  $D_{6h}$  to  $D_{2h}$  symmetry upon single ionization [34]. As previously done for oligoacenes [16a], the structural variations occurring in the charged species compared to the corresponding neutral one are expressed in Fig. 2 in terms of the percentage variations of the rotational constants A and B. These latter quantities are proportional to the inverse of the principal momenta of inertia in the plane of the molecule. Since rotational constants are here used just as a compact way to represent structural changes between different charge states, they were all computed at the optimized geometries, disregarding vibration–rotation coupling effects. Evaluating the differences of rotational constants between the charged species and the corresponding neutral counterparts,  $\Delta A$  and  $\Delta B$ , we thus computed the quantities  $A_{\text{rel}} = \Delta A/A_{\text{neutral}}$  and  $B_{\text{rel}} = \Delta B/B_{\text{neutral}}$ . Figure 2 shows that  $A_{\text{rel}}$  and  $B_{\text{rel}}$  display well-defined trends as a function of molecular size.

For oligoacenes and circumacenes the largest structural changes are observed for the anions, while the variations of cations are always small; in particular, the anions of both families appear to be primarily distorted along the long axis showing for all sizes a lengthening along it ( $B_{\text{rel}} < 0$ ) in comparison to the neutral molecules. The same holds true for both  $\pm 1$  charge–states of phenacenes, the cations showing also a sensible shortening along the short–axis ( $A_{\text{rel}} > 0$ ). In the case of oligorylenes, instead, at increasing molecular size the largest structural changes are observed for the cations, which appear to be primarily distorted along the long axis showing a shortening along it ( $B_{\text{rel}} > 0$ ).

#### 3.2 Ionization energies and electron affinities

The adiabatic and vertical values of electron affinities and ionization energies as obtained via total energy differences at the B3LYP/6-31+G\* level are given in Table 3 and displayed in Fig. 3 as a function of molecular size; for comparison, we report also the available experimental data [36]. In particular, the differences between computed and measured first ionization energies, under-

Table 3

Adiabatic and vertical values (within parentheses) of electron affinities and ionization energies of oligoacenes, phenacenes, circumacenes, and oligorylenes; all data, in eV, have been obtained via total energy differences at the B3LYP/6-31+G\* level. The experimental data are taken from the NIST Chemistry WebBook [36].

Molecule	Electron affinity		Ionization energy	
	Theory	Experiment	Theory	Experiment
Acenes ( $C_{4n+2}H_{2n+4}$ )				
naphthalene	-0.26(-0.38)	-0.20±0.05	7.80(7.89)	8.144±0.001
anthracene	0.53(0.43)	0.530±0.005	7.02(7.09)	7.439± 0.006
tetracene	1.08(1.00)	1.067±0.043	6.49(6.55)	6.97±0.05
pentacene	1.48(1.41)	1.392±0.043	6.12(6.16)	6.589±0.001
hexacene	1.78(1.72)	—	5.83(5.87)	6.36±0.02
Phenacenes ( $C_{4n+2}H_{2n+4}$ )				
phenanthrene	-0.05(-0.21)	0.01±0.04 <sup>a</sup>	7.53(7.63)	7.891±0.001
chrysene	0.29(0.19)	0.397±0.008	7.17(7.25)	7.60±0.01
picene	0.40(0.10)	0.542±0.008	7.04(7.13)	7.51±0.02
fulminene	0.57(0.48)	—	6.88(6.95)	7.36±0.02
7-phenacene	0.64(0.54)	—	6.80(6.87)	—
Circumacenes ( $C_{8n}H_{2n+6}$ )				
coronene	0.47(0.38)	0.470±0.090	7.02(7.08)	7.29±0.03
ovalene	1.17(1.11)	—	6.36(6.41)	6.71±0.01
circumanthracene	1.68(1.63)	—	5.90(5.94)	—
circumtetracene	2.06(2.02)	—	5.57(5.60)	—
circumpentacene	2.34(2.31)	—	5.33(5.35)	—
Rylenes ( $C_{10n}H_{4n+4}$ )				
perylene	0.96(0.87)	0.973±0.005	6.57(6.64)	6.960±0.001
terrylene	1.55(1.48)	—	5.98(6.05)	6.42±0.02
quaterrylene	1.91(1.85)	—	5.62(5.68)	6.11±0.02
pentarylene	2.17(2.11)	—	5.37(5.43)	—
hexarylene	2.37(2.31)	—	5.18(5.24)	—

<sup>a</sup> Taken from Ref. [37].

estimated by theory in all cases, are of the same order of magnitude as in previous analyses [23a,23k]: they increase systematically at increasing molecular size for each class (from  $\sim 4\%$  for naphthalene to  $\sim 10\%$  for hexacene, from  $\sim 5\%$  for phenanthrene to  $\sim 7\%$  for fulminene, from  $\sim 6\%$  for perylene to  $\sim 8\%$  for quaterrylene, and from  $\sim 4\%$  for coronene to  $\sim 5\%$  for ovalene). As already found in the literature [30] and confirmed in our benchmark calculations (see Sect. 2.1, Tables 1-2), these errors in the ionization energies can be largely corrected by range-separated functionals. On the contrary, as compared to ionization energies, the computed electron affinities are found to be in better agreement with experiments in all cases, confirming the very good performances of B3LYP/6-31+G\* to compute the electron affinities of PAHs [23b,23c,23i]. Oligoacenes display the largest variations for ionization energies and electron affinities as a function of molecular size. On the other hand, phenacenes show the smallest variations for the same properties. Circumacenes and oligorylenes behave in the same way at increasing sizes, with ionization energies reaching the value of about 5.2 eV and electron affinities

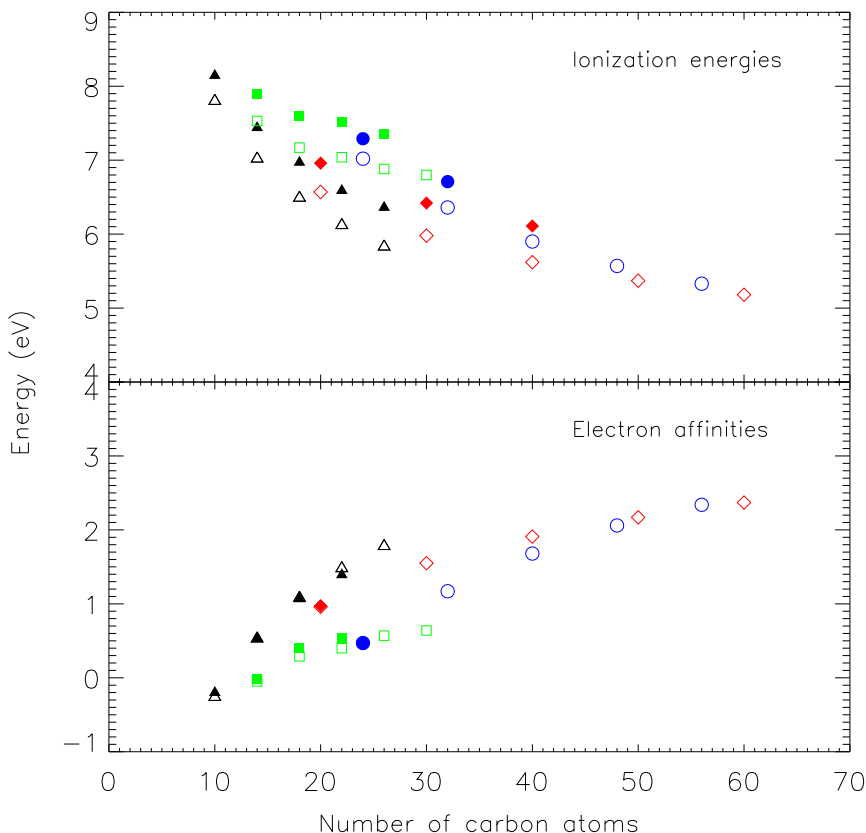


Fig. 3. Computed adiabatic ionization energies and electron affinities as a function of size for oligoacenes (black triangles), phenacenes (green squares), circumacenes (blue circles), and oligorylenes (red diamonds). When available, the corresponding experimental values are represented by the filled symbols (cfr. Table 3).

converging to about 2.4 eV.

### 3.3 HOMO–LUMO gap and excitonic effects

For each molecule considered, Table 4 compares the HOMO–LUMO gap  $E_{\text{gap}}^{\text{KS}}$  obtained as difference of Kohn–Sham eigenvalues, the excitation energy of the HOMO–LUMO transition  $E_{\text{gap}}^{\text{TD–DFT}}$  as given by frequency–space TD–DFT, and the corresponding experimental value  $E_{\text{gap}}^{\text{exp}}$ . In Table 4 we compare also the quasiparticle–corrected HOMO–LUMO gap computed via Eqs. (1) and (2) to the corresponding experimental value  $\text{QP}_{\text{gap}}^{\text{exp}} = I_{\text{exp}} - E_{\text{A,exp}}$  (cfr. Table 3). The theoretical exciton binding energy  $E_{\text{bind}}$  is estimated through the difference  $\text{QP}_{\text{gap}}^1 - E_{\text{gap}}^{\text{TD–DFT}}$ , and compared with its corresponding experimental value  $\text{QP}_{\text{gap}}^{\text{exp}} - E_{\text{gap}}^{\text{exp}}$ . For each class considered all of these quantities are displayed in Fig. 4 and, as expected due to a reduction of quantum confinement effects, they all decrease as a function of molecular size.

As shown in Table 4 and Fig. 4 in the case of oligoacenes the HOMO–LUMO gap obtained as difference between Kohn–Sham eigenvalues, with relative errors in the range 1–6%, gives a better description of the experimental optical gap as compared to TD–DFT. In the latter case, as already mentioned before, a system–size–dependent error is known to exist [23f], with a relative error increasing from 2 to 20% when going from naphthalene to hexacene. For circumacenes and oligorylenes the two methods have approximately the same accuracy in predicting the optical gap, with relative errors in the range 1–8%. On the contrary, TD–DFT results for phenacenes agree better with experiment (relative error 1–4%) than the corresponding Kohn–Sham gap (relative error 8–10%).

As previously discussed in Ref. [16a], the  $\Delta\text{SCF}$  QP–corrected HOMO–LUMO gaps of neutral oligoacenes compare very well with the DFT–based tight–binding GW data [39] but they are affected by similar errors as those found with TD–DFT. On the other hand, since these errors almost cancel each other in the evaluation of the exciton binding energy, we obtain an accurate estimate of  $E_{\text{bind}}$ . To the best of our knowledge the QP–corrected HOMO–LUMO gap for phenacenes, circumacenes, and oligorylenes have never been reported before in the literature. By comparing these values with the corresponding optical gap predicted by TD–DFT we could estimate the excitonic effects occurring in these molecules. We found in all cases appreciable excitonic effects due to both quantum confinement and reduction of screening;  $E_{\text{bind}}$  decreases as the size of the molecule increases with similar slope for the different families and approaches the value of about 1.6–1.8 eV for the largest species considered.

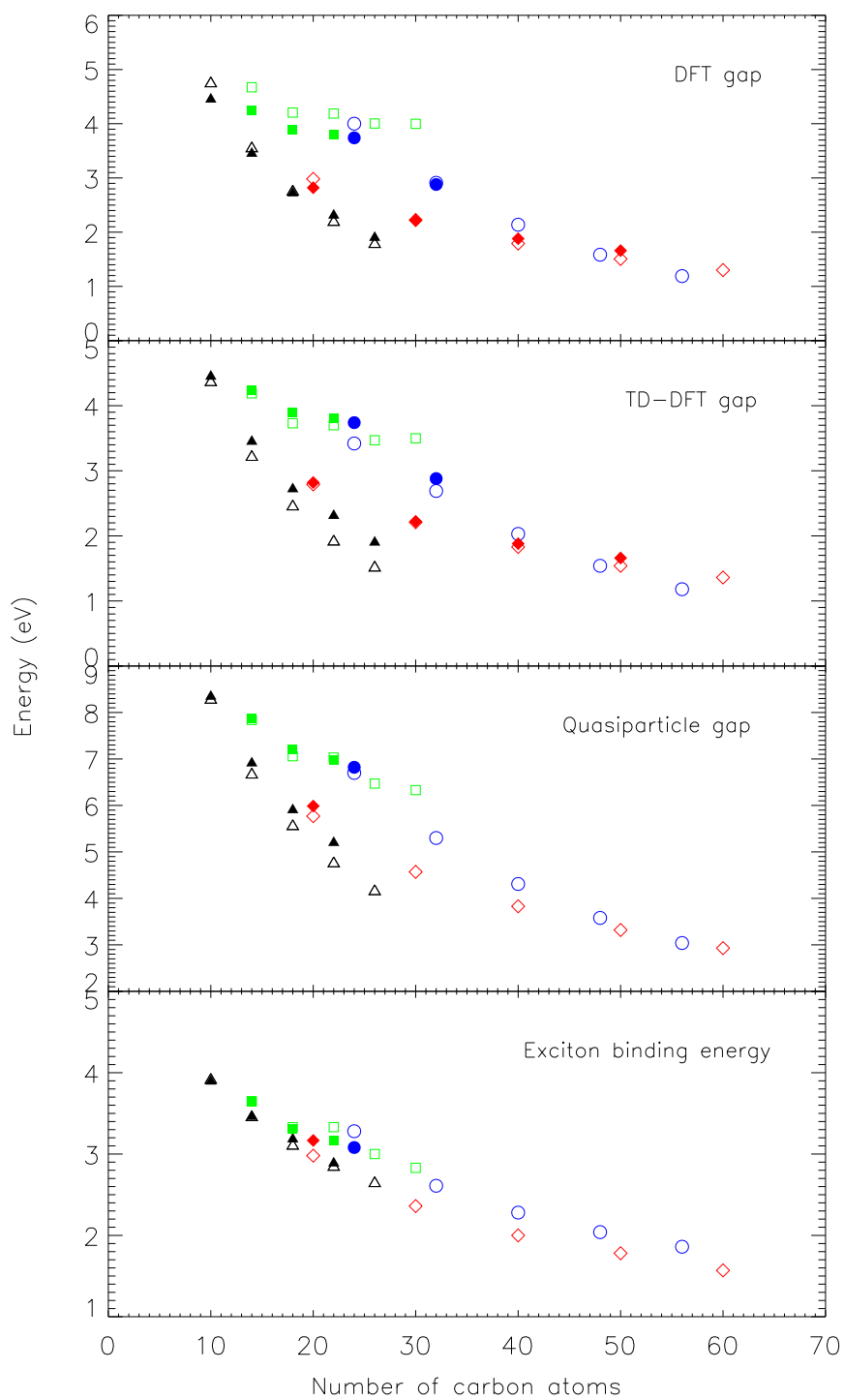


Fig. 4. Computed HOMO–LUMO, TD–DFT, and quasiparticle corrected energy gaps, and exciton binding energy as a function of molecular size for oligoacenes (black triangles), phenacenes (green squares), circumacenes (blue circles), and oligorylenes (red diamonds). When available, the corresponding experimental values are represented by the filled symbols (cfr. Table 4).

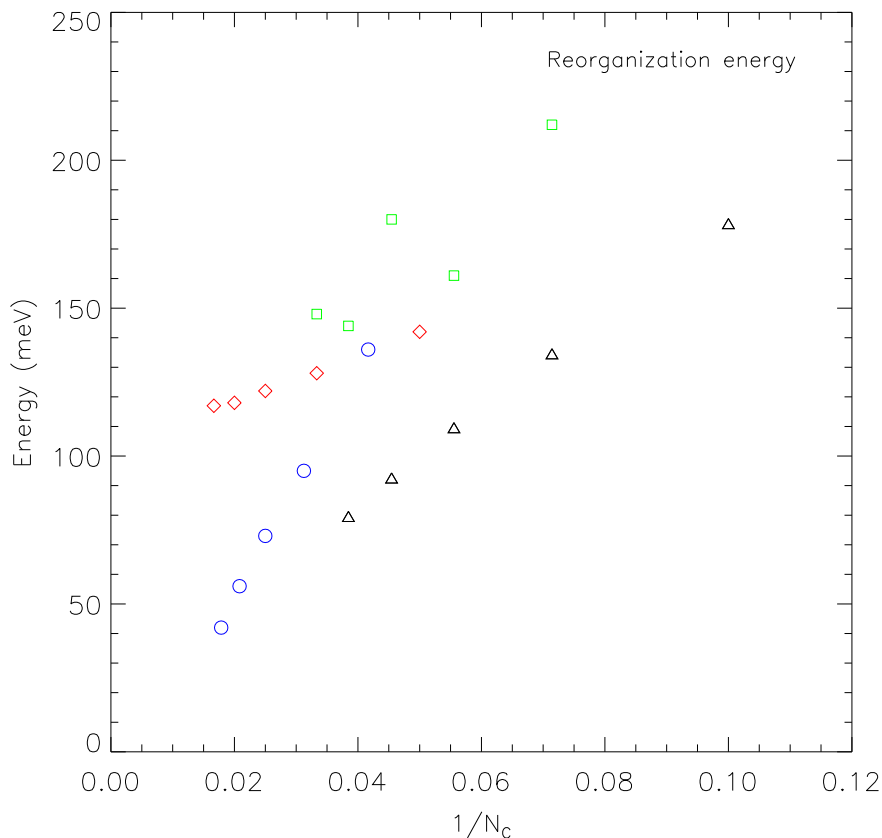


Fig. 5. Molecular reorganization energies computed using Eq. 3 for oligoacenes (black triangles), phenacenes (green squares), circumacenes (blue circles), and oligoarylenes (red diamonds), as a function of the inverse of the total number of carbon atoms  $N_C$ .

### 3.4 Molecular reorganization energies

The last row of Table 4 reports for each molecule the molecular reorganization energies  $\lambda$  obtained through Eq. 3. Our results for oligoacenes are in good agreement with previous DFT results [14a,14b]. Note that, while the performances of the B3LYP functional for the calculation of  $\lambda$  in conjugated materials can be improved by precisely calibrated DFT functionals [14b], its use in the present work is justified since it is expected to describe reasonably the differences between different families of PAHs. Due to strong electron-phonon coupling, the molecular reorganization energy  $\lambda$  is known to be inversely proportional to the total number of carbon atoms  $N_C$  [40]. Figure 5 confirms this general trend with the only exception of phenacenes, which display for  $\lambda$  an oscillatory behaviour like for the other physical properties computed (see Figs. 2-4). For the different families we observe a markedly different behaviour: while the reorganization energy of oligoarylenes decreases slowly as a function

of molecular size, circumacenes display a much more pronounced slope as compared to oligoacenes. These results are consistent with those previously found in Ref. [2b], and confirm that circumacenes are indeed good candidates for new emerging technologies.

Table 4

Comparison between HOMO–LUMO gap, TD–DFT excitation energy of the HOMO–LUMO transition, quasi–particle corrected gap, and molecular reorganization energy for the PAHs considered. All data have been obtained at the B3LYP/6–31+G\* level of theory.

Molecule (formula)	$E_{\text{gap}}^{\text{KS}}$	$E_{\text{gap}}^{\text{TD-DFT}}$	$E_{\text{gap}}^{\text{exp}}$	$\text{QP}_{\text{gap}}^1$	$\text{QP}_{\text{gap}}^2$	$\text{QP}_{\text{gap}}^{\text{exp}}$	$E_{\text{bind}}$	$E_{\text{bind}}^{\text{exp}}$	$\lambda$
naphthalene (C <sub>10</sub> H <sub>8</sub> )	4.74	4.36	4.45 <sup>a</sup>	8.27	8.12	8.34	3.91	3.89	0.178
anthracene (C <sub>14</sub> H <sub>10</sub> )	3.54	3.21	3.45 <sup>a</sup>	6.66	6.58	6.91	3.45	3.46	0.134
tetracene (C <sub>18</sub> H <sub>12</sub> )	2.74	2.45	2.72 <sup>a</sup>	5.55	5.50	5.90	3.10	3.18	0.109
pentacene (C <sub>22</sub> H <sub>14</sub> )	2.19	1.91	2.31 <sup>a</sup>	4.75	4.72	5.20	2.84	2.89	0.092
hexacene (C <sub>26</sub> H <sub>16</sub> )	1.78	1.51	1.90 <sup>a</sup>	4.15	4.13	—	2.64	—	0.079
phenanthrene (C <sub>14</sub> H <sub>10</sub> )	4.67	4.19	4.24 <sup>b</sup>	7.84	7.44	7.88	3.65	3.64	0.212
chrysene (C <sub>18</sub> H <sub>12</sub> )	4.21	3.73	3.89 <sup>b</sup>	7.06	7.00	7.20	3.33	3.31	0.161
picene (C <sub>22</sub> H <sub>14</sub> )	4.19	3.70	3.80 <sup>b</sup>	7.03	6.82	6.97	3.33	3.17	0.180
fulminene (C <sub>26</sub> H <sub>16</sub> )	4.00	3.47	—	6.47	6.42	—	3.00	—	0.144
7–phenacene (C <sub>30</sub> H <sub>18</sub> )	4.00	3.50	—	6.33	6.26	—	2.83	—	0.148
coronene (C <sub>24</sub> H <sub>12</sub> )	4.00	3.42	3.74 <sup>c</sup>	6.70	6.64	6.82	3.28	3.08	0.136
ovalene (C <sub>32</sub> H <sub>14</sub> )	2.91	2.69	2.88 <sup>c</sup>	5.30	5.28	—	2.61	—	0.095
circumanthracene (C <sub>40</sub> H <sub>16</sub> )	2.14	2.03	—	4.31	4.30	—	2.28	—	0.073
circumtetracene (C <sub>48</sub> H <sub>18</sub> )	1.58	1.54	—	3.58	3.58	—	2.04	—	0.056
circumpentacene (C <sub>56</sub> H <sub>20</sub> )	1.19	1.18	—	3.04	3.04	—	1.86	—	0.042
perylene (C <sub>20</sub> H <sub>12</sub> )	2.98	2.79	2.82 <sup>d</sup>	5.77	5.71	5.99	2.98	3.17	0.142
terrylene (C <sub>30</sub> H <sub>16</sub> )	2.22	2.21	2.22 <sup>d</sup>	4.57	4.53	—	2.36	—	0.128
quaterrylene (C <sub>40</sub> H <sub>20</sub> )	1.79	1.83	1.88 <sup>d</sup>	3.83	3.81	—	2.00	—	0.122
pentarylene (C <sub>50</sub> H <sub>24</sub> )	1.51	1.54	1.66 <sup>d</sup>	3.32	3.30	—	1.78	—	0.118
hexarylene (C <sub>60</sub> H <sub>28</sub> )	1.30	1.36	—	2.93	2.92	—	1.57	—	0.117

<sup>a</sup> See compilation in Ref. [16a]. <sup>b</sup> From Ref. [23e]. <sup>c</sup> From Ref. [38]. <sup>d</sup> From Ref. [12].

### 3.5 Absorption spectra

Figures 6-8 display the absorption spectra of each of the molecule considered, in its neutral and  $\pm 1$  charge-state, as computed using the real-time real-space TD-DFT implementation [35a,35b]. Note that the spectra of the higher neutral and singly-charged phenacenes, circumacenes, and oligorylenes, have never been reported before. This enabled a quantitative comparison of the absorption in the visible part of the spectrum for each class, which gives an estimate of its potential use as photo-active element in opto-electronic devices. To this end Fig. 9 shows the integrated values in the range 1.0–3.0 eV of the individual dipole strength-functions  $S(E)$  (see Eq. 5) divided by the total number of carbon atoms in each molecule as a function of molecular size.

As expected from previous analyses [16a,16b], with the exception of the different intensities which are related to the total number of electrons in the molecule, all of the spectra in Figs. 6-8 display a similar broad excitation peaking at  $\sim 17$ – $18$  eV, which involves  $\pi \rightarrow \sigma^*$ ,  $\sigma \rightarrow \pi^*$ ,  $\sigma \rightarrow \sigma^*$ , and Rydberg spectral transitions, and which is relatively insensitive to the charge-state of the molecule. Note that we already showed [16a,16b] our results to be in good agreement up to photon energies of about 30 eV with the experimental data obtained for a few neutral PAHs [38]. However, the use of a finite simulation box in our simulations does not give a satisfactory treatment of continuum effects in this spectral window and produces spurious structures as compared to experiments [16a,16b].

The main differences among families arise in the low-energy part of the spectrum, from the near-IR to the near-UV up to about 8 eV, which involves electronic transitions of  $\pi \rightarrow \pi^*$  character. This is also the spectral window which is more interesting from an applicative point of view. In particular, an inspection of Fig. 6 shows that each family displays a continuous redshift of the absorption at increasing sizes. This behaviour was expected as a consequence of the continuous decrease in bandgap already observed for each class (see Fig. 4). As to the charged species, as shown in Figs. 7–8 we found that PAH radical cations and anions display intense optical transitions at lower energies than their parent molecule, and have very similar electronic spectra. These findings, already known for charged PAHs from extensive spectroscopic studies in frozen glassy organic solids [41a,41b], are in qualitative agreement with the particle-hole equivalence in the pairing theorem of Hückel’s theory.

The behaviour described above at low energies translates for each molecule in each class into a systematic increase of the integrated strength-function in the range 1.0–3.0 eV when going from the neutral to the cation and anion (see Fig. 9). This effect is more pronounced for oligoacenes and phenacenes and, as expected, the observed scatter between the different charge-states

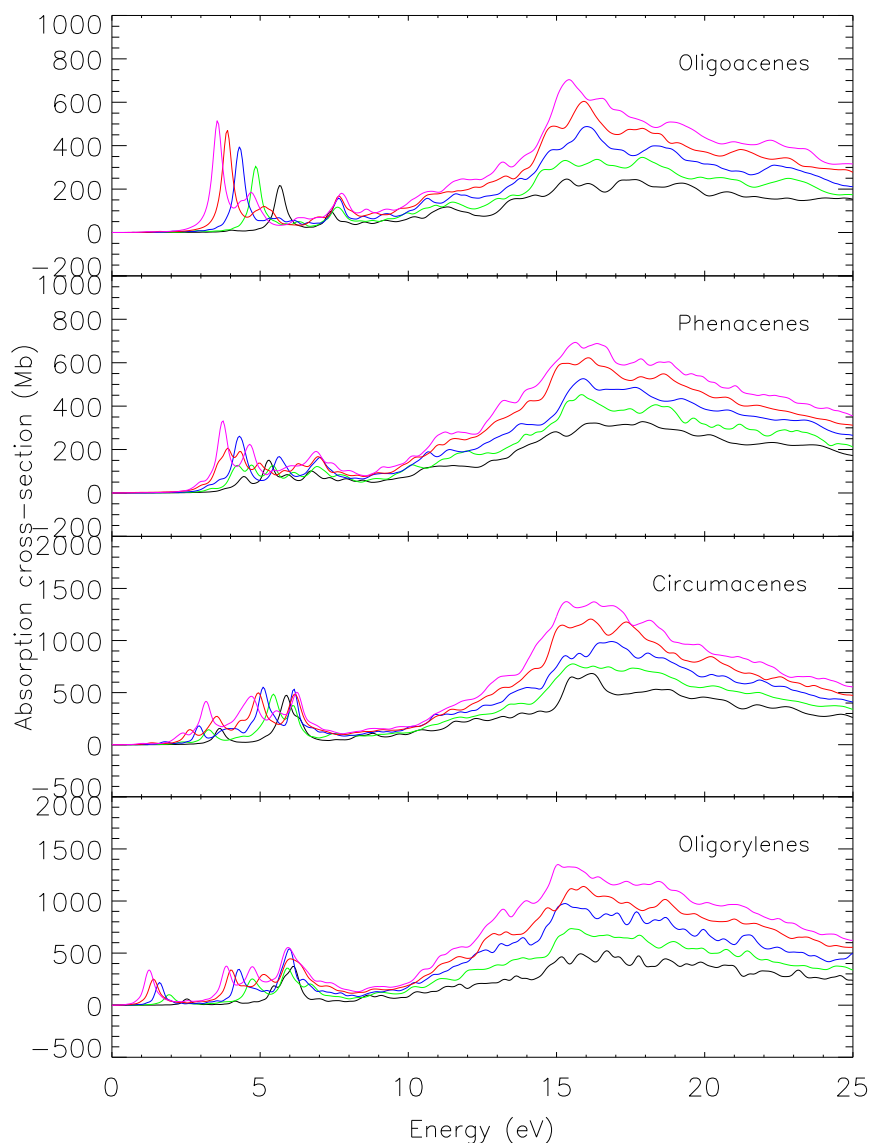


Fig. 6. Electronic absorption spectra of the neutral molecules of the four PAH classes considered, as computed using the real-time real-space TD-DFT implementation of the OCTOPUS code.

decreases with increasing molecular size. Interestingly, oligorylenes appear to be much more efficient in absorbing low-energy photons in comparison to the other classes; as an example, focusing on the neutral species with the same number of carbon atoms, the value of  $S(E)/N_C$  for quaterrylene exceeds by more than 80% the corresponding value for circumanthracene. Since red photons represent a significant portion of the solar energy, this result might have important technological implications.

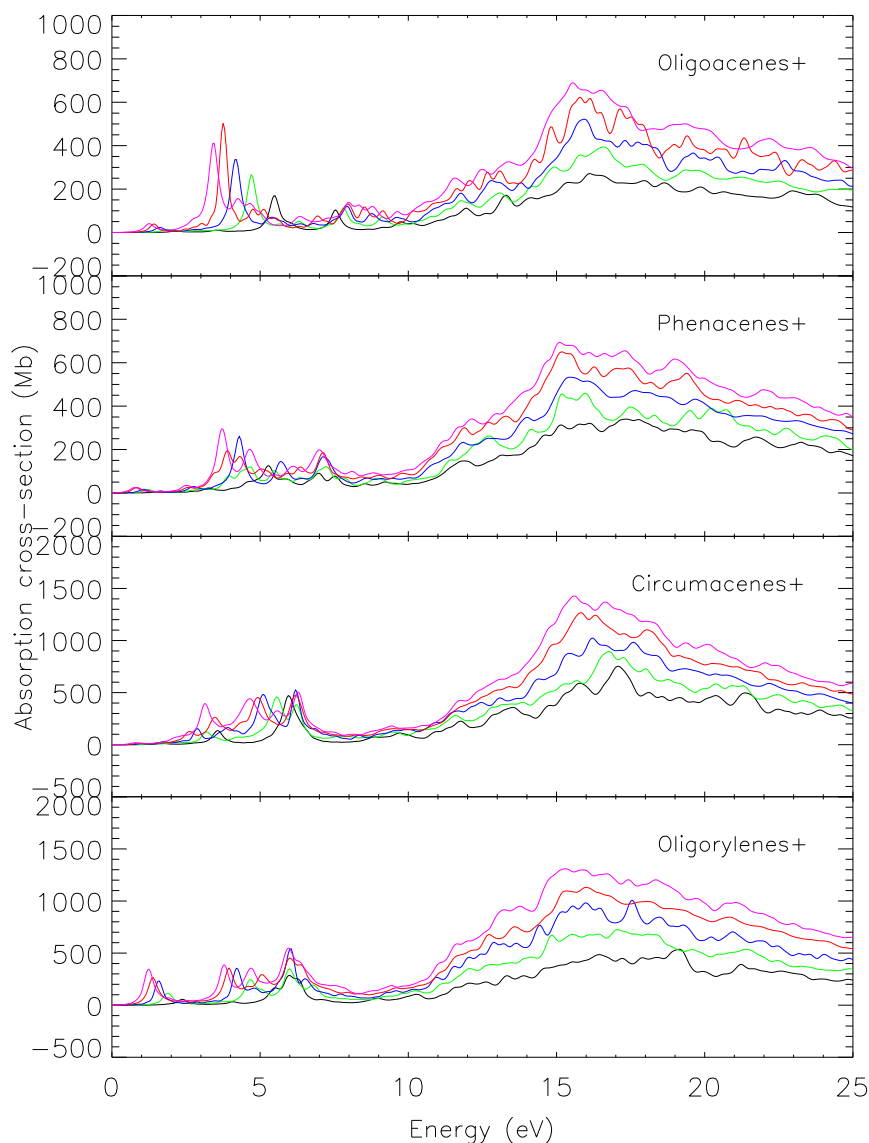


Fig. 7. Same as Fig. 6 for the corresponding cations.

#### 4 Concluding remarks

We presented a systematic theoretical study of the five smallest species of oligoacenes, phenacenes, circumacenes, and oligorylenes in their -1, 0, and +1 charge-states. From the ground-state structural relaxations performed at the B3LYP/6-31+G\* level we computed the electron affinities, the first ionization energies, the molecular reorganization energies, and the quasiparticle correction to the HOMO-LUMO energy gap. We found good agreement with the available experimental data as well as with previous theoretical results. Benchmark calculations performed using the range-separated functional LC-BLYP

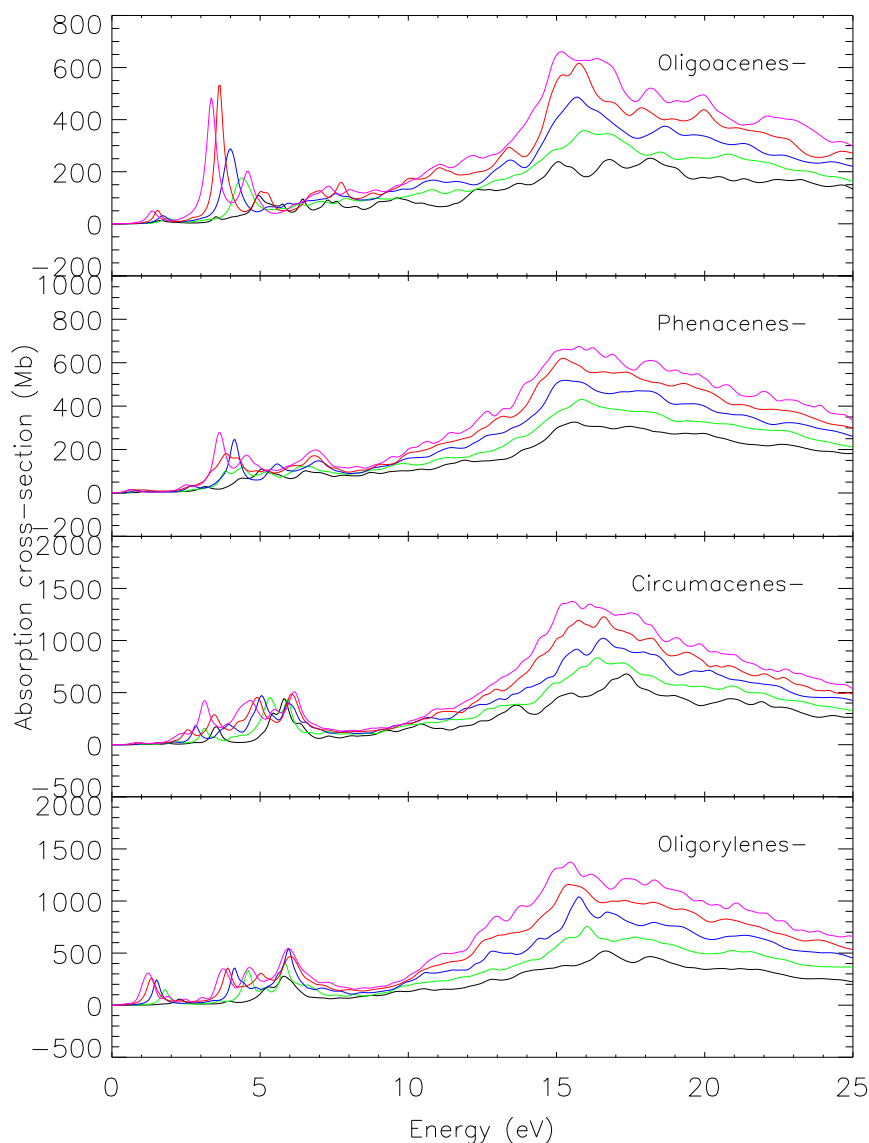


Fig. 8. Same as Fig. 6 for the corresponding anions.

suggest that the agreement with the experiment can be further improved for some selected properties (e. g. the ionization energy); a systematic study will be the subject of future work. Concerning transport properties, circumacenes appear to have the most favorable properties for technological applications, displaying a steeper decrease of the molecular reorganization energy as the molecular size increases. We computed also the electronic absorption spectra using a compendium of the TD-DFT theoretical framework in both frequency space, to obtain the optical gap and thus estimate the exciton binding energy, and real-time real-space, to obtain in a single step the whole photo-absorption cross-section extending up to the far-UV. The results of this latter method, in particular, enabled a close comparison between the families considered with

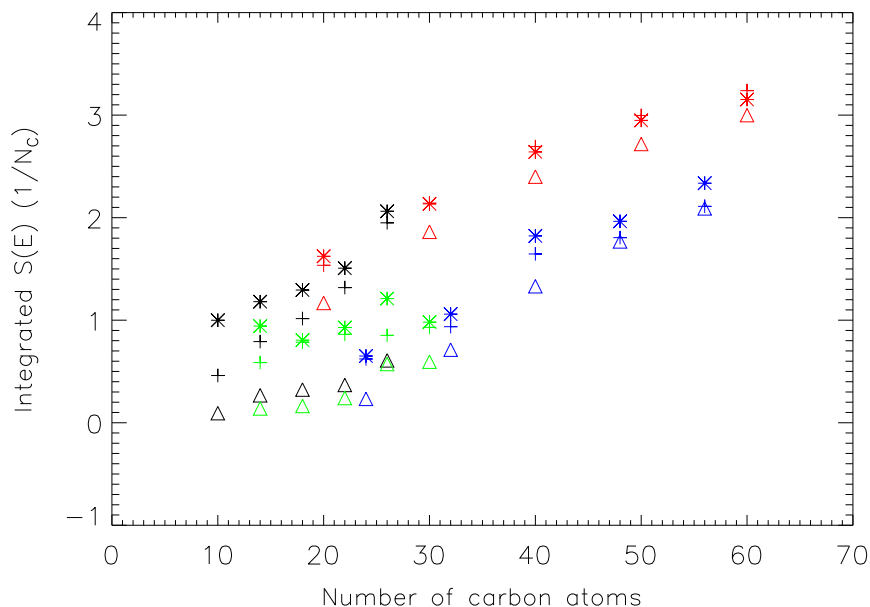


Fig. 9. Comparison between the integrated values in the range 1.0–3.0 eV of the individual dipole strength–functions  $S(E)$  (see Eq. 5) divided by the total number of carbon atoms  $N_C$  for the anions (asterisks), neutrals (triangles), cations (crosses) of oligoacenes (black), phenacenes (green), circumacenes (blue), and oligorylenes (red) as a function of molecular size.

respect to their potential use as photoactive materials in opto–electronic devices. Overall, oligorylenes appear to be much more efficient in absorbing visible light and red photons in particular, which might have important technological implications in the field of photovoltaics.

## Acknowledgements

This work has been funded by the Italian Institute of Technology (IIT) under Project SEED “POLYPHEMO”. We acknowledge computational support by CYBERSAR (Cagliari, Italy) and CASPUR (Rome, Italy). G. C. acknowledges financial support from IDEA–AISBL.

## References

- [1a] R. F. Curl, *Nature* 363 (1993) 14.
- [1b] C. J. Pope, J. A. Marr, J. B. Howard, *J. Phys. Chem.* 97 (1993) 11001.

- [2a] D. Jiang, S. Dai, *Chem. Phys. Lett.* 466 (2008) 72
- [2b] J. C. Sancho-García, A. J. Pérez-Jiménez, *Phys. Chem. Chem. Phys.* 11 (2009) 2741.
- [3a] A. Lunch, *The Carcinogenic Effects of Polycyclic Aromatic Hydrocarbons*, London: Imperial College Press, 2005.
- [3b] M. Rehwagen, A. Müller, L. Massolo, O. Herbarth, A. Ronco, *Science of the Total Environment* 348 (2005), 199.
- [4a] A. G. G. M. Tielens, *The Physics and Chemistry of the Interstellar Medium*, Cambridge: Cambridge University Press, 2005.
- [4b] A. G. G. M. Tielens, *Interstellar Polycyclic Aromatic Hydrocarbon Molecules*, *Annual Review of Astronomy & Astrophysics* 46 (2008) 289.
- [5] J. E. Anthony, *Angew. Chem. Int. Ed.* 47 (2008) 452.
- [6] M. Halik, H. Klauk, U. Zschieschang, T. Kriem, G. Schmid, W. Radlik, K. Wussow, *Appl. Phys. Lett.* 81 (2002) 289.
- [7] Y. Kan, L. Wang, L. Duan, Y. Hu, G. Wu, Y. Qiu, *Appl. Phys. Lett.* 84 (2004) 1513.
- [8] S. Yoo, B. Domercq, B. Kippelen, *Appl. Phys. Lett.* 85 (2004) 5427.
- [9] I. Shiyankovskaya, K. D. Singer, V. Percec, T. K. Bera, Y. Miura, M. Glodde, *Phys. Rev. B* 67 (2003) 035204.
- [10a] J. E. Anthony, *Chem. Rev.* 106 (2006) 5028.
- [10b] A. R. Murphy, J. M. J. Fréchet, *Chem. Rev.* 107 (2007) 1066.
- [10c] L. Huang, D. Rocca, S. Baroni, K. E. Gubbins, M. Buongiorno Nardelli, *J. Chem. Phys.* 130 (2009) 194701.
- [10d] S. Karak, V.S. Reddy, S. K. Ray, A. Dhar, *Org. Electron.* 10 (2009) 1006.
- [10e] F. De Angelis, *Chem. Phys. Lett.* 493 (2010) 323.
- [11] F. B. Mallory, K. E. Butler, A. C. Evans, E. J. Brondyke, C. W. Mallory, C. Yang, A. Ellenstein, *J. Am. Chem. Soc.* 119 (1997) 2119.
- [12] S. Karabunarliev, M. Baumgarten, K. Mllen, *J. Phys. Chem. A* 102 (1998) 7029.
- [13] A. J. Pérez-Jiménez and J. C. Sancho-García, *J. Am. Chem. Soc.* 131 (2009) 14857.
- [14a] J.-L. Brédas, D. Beljonne, V. Coropceanu, J. Cornil, *Chem. Rev.* 104 (2004) 4971.
- [14b] J. C. Sancho-García, *Chem. Phys.* 331 (2007) 321.
- [15] G. Mallocci, C. Joblin, G. Mulas, *Chem. Phys.* 332 (2007) 353.

- [16a] G. Mallocci, G. Mulas, G. Cappellini, C. Joblin, *Chem. Phys.* 340 (2007) 43.
- [16b] G. Cappellini, G. Mallocci, G. Mulas, *Superlattices and Microstructures* 46 (2009) 14.
- [17a] R. W. Godby, M. Schlüter, L. J. Sham, *Phys. Rev. B* 37 (1988) 10159.
- [17b] R. O. Jones, O. Gunnarsson, *Rev. Mod. Phys.* 61 (1989) 689.
- [17c] R. M. Dreizler, E. K. U. Gross, *Density Functional Theory*, Berlin: Springer, 1990.
- [17d] A. Görling, *Phys. Rev. A* 54 (1996) 3912.
- [18a] S. Hirata, M. Head-Gordon, *Chem. Phys. Lett.* 302 (1999) 375.
- [18b] K. Yabana, G. F. Bertsch, *Int. J. Quant. Chem.* 75 (1999) 55.
- [18c] M. A. L. Marques, E. K. U. Gross, *Ann. Rev. Phys. Chem.* 55 (2004) 3425.
- [18d] A. Dreuw, M. Head-Gordon, *Chem. Rev.* 105 (2005) 4009.
- [19] M. Valiev, E.J. Bylaska, N. Govind, K. Kowalski, T.P. Straatsma, H.J.J. van Dam, D. Wang, J. Nieplocha, E. Apra, T.L. Windus, W.A. de Jong, *Comput. Phys. Commun.* 181 (2010) 1477.
- [20] A. D. Becke, *J. Chem. Phys.* 98 (1993) 5648.
- [21] C. Lee, W. Yang, R. Parr, *Phys. Rev. B* 37 (1988) 785.
- [22a] J. M. L. Martin, J. El-Yazal, J. Francois, *J. Phys. Chem.* 100 (1996) 15358.
- [22b] S. R. Langhoff, *J. Phys. Chem* 100 (1996) 2819.
- [23a] K. B. Wiberg, *J. Org. Chem.* 62 (1997) 5720.
- [23b] C. E. H. Dessent, *Chem. Phys. Lett.* 330 (2000) 180.
- [23c] J. C. Rienstra-Kiracofe, C. J. Barden, S. T. Brown, H. F. Schaefer III, *J. Phys. Chem. A* 105 (2001) 524.
- [23d] K. A. Nguyen, J. Kennel, R. Pachter, *J. Chem. Phys.* 117 (2002) 7128.
- [23e] M. Parac, S. Grimme, *Chem. Phys.* 292 (2003) 11.
- [23f] S. Grimme, M. Parac, *Chem. Phys. Chem.* 3 (2003) 292.
- [23g] M. S. Deleuze, L. Claes, E. S. Kryachko, J.-P. François, *J. Chem. Phys.* 119 (2003) 3106.
- [23h] M. Dierksen, S. Grimme, *J. Chem. Phys.* 120 (2004) 3544.
- [23i] G. Mallocci, G. Mulas, G. Cappellini, V. Fiorentini, I. Porceddu, *A&A* 432 (2005) 585.
- [23j] T. Kato, T. Yamabe, *Chem. Phys. Lett.* 403 (2005) 113.

- [23k] E. S. Kadantsev, M. J. Stott, A. Rubio, *J. Chem. Phys.* 124 (2006) 134901.
- [24a] R. Bauernschmitt, R. Ahlrichs, *Chem. Phys. Lett.* 256 (1996) 454.
- [24b] K. B. Wiberg, R. E. Stratmann, M. J. Frish, *Chem. Phys. Lett.* 297 (1998) 60.
- [25a] S. Hirata, M. Head-Gordon, *Chem. Phys. Lett.* 302 (1999) 375.
- [25b] S. Hirata, M. Head-Gordon, *Chem. Phys. Lett.* 314 (1999) 291.
- [26a] M. E. Casida, C. Jamorski, K. C. Casida, D. Salahub, *J. Chem. Phys.* 108 (1998), 4439.
- [26b] D. J. Tozer, N. C. Handy, *J. Chem. Phys.* 109 (1998) 10180.
- [26c] N. C. Handy, D. J. Tozer, *J. Comput. Chem.* 20 (1999) 106.
- [27a] R. J. Cave, F. Zhang, N. T. Maitra, K. Burke, *Chem. Phys. Lett.* 389 (2004) 39.
- [27b] N. T. Maitra, F. Zhang, R. J. Cave, K. Burke, *J. Chem. Phys.* 120 (2004) 5932.
- [28a] D. J. Tozer, R. D. Amos, N. C. Handy, B. O. Roos, L. Serrano-Andres, *Mol. Phys.* 97 (1999) 859.
- [28b] A. L. Sobolewski, W. Domcke, *Chem. Phys.* 294 (2003) 73.
- [28c] A. Dreuw, M. Head-Gordon, *J. Am. Chem. Soc.* 126 (2004) 4007.
- [29] Z.-L. Cai, K. Sendt, J. R. Reimers, *J. Chem. Phys.* 117 (2002) 5543.
- [30] B. M. Wong, T. H. Hsieh, *J. Chem. Theory Comput.* 6 (2010) 3704.
- [31a] H. Iikura, T. Tsuneda, T. Yanai, K. Hirao, *J. Chem. Phys.* 115 (2001) 3540.
- [31b] Y. Tawada, T. Tsuneda, S. Yanagisawa, T. Yanai, K. Hirao, *J. Chem. Phys.* 120 (2004) 8425.
- [31c] M. Kamiya, H. Sekino, T. Tsuneda, K. Hirao, *J. Chem. Phys.* 122 (2005) 234111.
- [31d] T. Sato, T. Tsuneda, K. Hirao, *J. Chem. Phys.* 126 (2007) 234114.
- [32a] D. Jacquemin, E. A. Perpète, G. Scalmani, M. J. Frisch, R. Kobayashi, C. Adamo, *J. Chem. Phys.* 126 (2007) 144105.
- [32b] D. Jacquemin, E. A. Perpète, O. A. Vydrov, G. E. Scuseria, C. Adamo, *J. Chem. Phys.* 127 (2007) 094102.
- [32c] D. Jacquemin, E. A. Perpète, G. E. Scuseria, I. Ciofini, C. Adamo, *J. Chem. Theory Comput.* 4 (2008) 123.
- [32d] D. Jacquemin, V. Wathelet, E. A. Perpète, C. Adamo, *J. Chem. Theory Comput.* 5 (2009) 2420.

- [32e] B. M. Wong, M. Piacenza, F. Della Sala, *Phys. Chem. Chem. Phys.* 11 (2009) 4498.
- [33a] S.J. Vosko, L. Wilk, M. Nusair, *Can. J. Phys.* 58 (1980) 1200.
- [33b] J.P. Perdew, K. Burke, M. Ernzerhof, *Phys. Rev. Lett.* 77 (1996) 3865.
- [34] T. Kato, K. Yoshizawa, T. Yamabe, *J. Chem. Phys.* 110 (1999) 249.
- [35a] A. Castro, M. A. L. Marques, J. A. Alonso, G. F. Bertsch, K. Yabana, A. Rubio, *J. Chem. Phys.* 116 (2002) 1930.
- [35b] M. A. L. Marques, A. Castro, G. F. Bertsch, A. Rubio, *Comp. Phys. Comm.* 151 (2003) 60.
- [36] S. Lias, Ionization energy evaluation, in: P. J. Linstrom, W. G. Mallard (Eds.), *NIST Chemistry WebBook, NIST Standard Reference Database Number 69*, National Institute of Standards and Technology - <http://webbook.nist.gov>, Gaithersburg MD, 2005.
- [37] M. Tschurl, U. Boesl, S. Gilb, *J. Chem. Phys.* 125 (2006) 194310.
- [38] C. Joblin, Ph.D. thesis, Université Paris 7 (1992).
- [39] T. A. Niehaus, M. Rohlfing, F. della Sala, A. di Carlo, T. Frauenheim, *Phys. Rev. A* 71 (2005) 022508-1.
- [40] A. Devos, M. Lannoo, *Phys. Rev. B* 58 (1998) 8236
- [41a] T. Shida, S. Iwata, *J. Am. Chem. Soc.* 95 (1973) 3473.
- [41b] T. Shida, *Electronic absorption spectra of radical ions*, Amsterdam: Elsevier, 1988.